JOURNAL OF APPLIED POLYMER SCIENCE VOL. 18, PP. 3279-3304 (1974)

Studies on Melt Spinning. IV. On the Stability of Melt Spinning

SUSUMU KASE, *Technical Department,*
Toyobo Co. Ltd., Kitaku Dojima, Osaka 530, Japan

Synopsis

The stability of melt spinning has been studied theoretically by solving for transients the perturbed form of the simultaneous partial differential equations of melt spinning introduced by the author in a previous study. Computed stability limits summarized in the form of maps in the (t^*—St) plane with the cooling air speed serving as the third parameter showed that the thread must be in a molten state at the take-up before an instability can develop and that the cooling of the thread by air plays a predominant role in stabilizing the melt spinning. Here, t^* is air temperature and St is the Stanton number. Draw resonances were observed experimentally in a water-quenched melt spinning of PET fiber and in the casting of PP film. Experimental results agreed well with theoretical simulations with respect to oscillation periods and stability. Draw resonance observed by Bergonzoni et al. was closely simulated by means of the present theories.

INTRODUCTION

Instabilities never develop in conventional air-quenched melt spinning of PET, PP, or nylon fibers. It does not follow, however, that melt spinning is always stable. It does become unstable under certain special spinning conditions resulting in clearly periodic and very large variations in the thickness of thread taken up. This phenomenon has been called the draw resonance ever since Miller[1] used the term. It just happens that conventional melt spinning is always carried out under stable operating conditions.

The author[2,3] previously developed simultaneous partial differential equations which simulate the dynamics of melt spinning and subsequently used the equations in simulating the draw resonance encountered in the casting of PP film.[4]

Thereafter, Shah and Pearson[5,6] studied extensively the stability of melt spinning starting from partial differential equations essentially identical to the author's and developed stability criteria for Newtonian liquids under isothermal and nonisothermal spinning conditions. Their studies[7,8] have been extended to include power law fluids and the effects of surface tension, inertia, etc. However, experiments are lacking in their research and the significance of cooling on the stability of melt spinning has not been discussed in detail.

In the present study, the simultaneous partial differential equations of melt spinning are first expanded into perturbation equations around the steady-state solutions, the perturbation equations are solved for transients under many different parameter values, and the derived stability limits are summarized in the form of maps in the (t^* − St) plane for the purpose of discussing in detail the effects of cooling on the spinning stability, where t^* is the air temperature and St is the Stanton number which is a measure of spinning flow rate.

A semianalytical solution of the perturbation equations is sought for the case of isothermal spinning to enable the prediction of oscillation period from a given spinning condition.

Theoretical findings are then compared with experimentally observed draw resonance in a water-quenched melt spinning of PET and in the casting of PP film which is a two-dimensional melt spinning. Draw resonance in the extrusion of thick PP ribbons observed by Bergonzoni et al.[9] is also simulated by means of the above solution for the isothermal spinning.

SIMULTANEOUS PARTIAL DIFFERENTIAL EQUATIONS OF MELT SPINNING AND THEIR PERTURBATION EQUATIONS

The author introduced in a previous study a set of simultaneous partial differential equations (1) through (3). Equations (4) and (5) are expressions respectively for the coefficient of heat transfer at the thread surface and the Trouton viscosity β of the polymer:

$$\frac{\partial v}{\partial x} = \frac{F}{A\beta} \tag{1}$$

$$\frac{\partial A}{\partial \tau} + v\frac{\partial A}{\partial x} = -A\frac{\partial v}{\partial x} \tag{2}$$

$$\frac{\partial t}{\partial \tau} + v\frac{\partial t}{\partial x} = \frac{2\sqrt{\pi}h(t^* - t)}{\rho C_p A} \tag{3}$$

$$h = 0.473 \times 10^{-4} A^{-0.333} v_y^{0.333} \left[1 + \left(8\frac{v_y}{v}\right)^2\right]^{0.167} \tag{4}$$

$$\beta = \beta_\infty \left[e^{E/(t + 273)} + \frac{R}{t - 60}\right] \tag{5}$$

where v, A, and t respectively are velocity, cross-sectional area, and temperature of the thread at time τ and distance x from the spinneret; ρ, C_p, and E are respectively density, specific heat, and activation energy of polymer; and v_y is the cooling air speed in the horizontal direction. Thread tension F is assumed independent of x and is determined to satisfy the boundary condition at the take-up. The second term on the right-hand side of eq. (5) takes into account the complete solidification of polymer at a certain temperature, which in this case is 60°C (see Fig. 1).

Major simplifying assumptions made in introducing eqs. (1) through (5) are (i) round thread cross section; (ii) flat velocity and temperature pro-

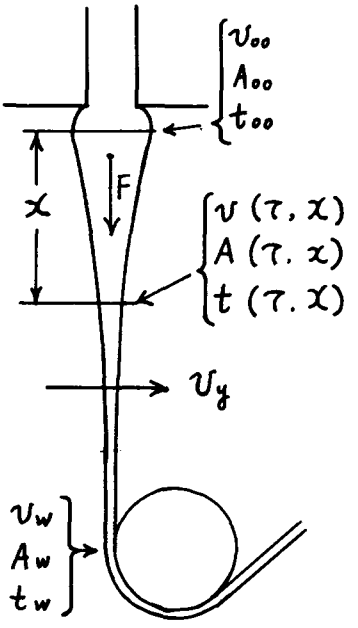

Fig. 1. Diagram of melt spinning.

files across the thread; (iii) Newtonian viscosity; and (iv) negligibility of air drag force, gravity force, and surface tension. Steady-state solutions of eqs. (1) through (3) are hereafter designated by using subscript 0 and are simply called steady-state solutions.

The author[3] has linearized eqs. (1) through (3) by considering the perturbation about the steady-state solutions:

$$0 = -\frac{\partial \bar{v}}{\partial z} - f_1\bar{v} - f_1\bar{A} + f_2\bar{l} + f_1\bar{F} \tag{6}$$

$$\frac{\partial \bar{A}}{\partial \tau} = -\frac{\partial \bar{v}}{\partial z} - \frac{\partial \bar{A}}{\partial z} \tag{7}$$

$$\frac{\partial \bar{l}}{\partial \tau} = -\frac{\partial \bar{l}}{\partial z} + f_4\bar{v} + f_3\bar{A} + f_6\bar{l} - f_5\bar{v}_y \tag{8}$$

where

$$v = v_0(z)[1 + \bar{v}(z,\tau)] \tag{9}$$

$$A = A_0(z)[1 + \bar{A}(z, \tau)] \tag{10}$$

$$t = t_0(z)[1 + \bar{l}(z,\tau)] \tag{11}$$

$$F = F_0[1 + F(\tau)] \tag{12}$$

$$x_y = x_{y0}(z)[1 + \bar{v}_y(z, \tau)] \tag{13}$$

$$\int_0^x \frac{dx}{v_0(x)} = z. \tag{14}$$

Coefficients f_1 through f_6 are functions of z and are given in the previous paper,[3] except that

$$f_6 = \frac{1}{t_0 - t^*} \frac{dt^*}{dz}. \tag{15}$$

It can be shown that f_1 through f_6 are completely fixed whenever the values of steady-state solutions $v_0(z)$, $A_0(z)$, and $t_0(z)$ are fixed.

It should be noted that under a steady state, eq. (2) can be readily integrated to give

$$G_0 = \rho A_0 v_0 \tag{16}$$

where G_0 is the steady-state mass flow rate.

In solving the perturbation equations (6) through (8) for transients, the following boundary conditions are used: (i) $\bar{v} = \bar{A} = \bar{t} = 0$ at the spinneret ($z = 0$); (ii) $\bar{v} = \bar{A} = \bar{t} = 0$ at time zero ($\tau = 0$); and (iii) stepwise change in take-up speed:

$$\bar{v}_w = u(\tau) = \text{unit step function} \tag{17}$$

where subscript w signifies a value at the take-up point.

Hereafter, transient solutions of perturbation equations (6) through (8) are simply called transient solutions.

NUMERICAL SOLUTION OF PERTURBATION EQUATIONS

After testing three different numerical schemes, a simple backward difference along the characteristic curves of the perturbation equations was selected for the numerical solution, for it gave the most smooth solution free of irregular spikes.

When integers i and j denote respectively the ith increment in variable z and the jth increment in time τ, the perturbation equations are converted into difference equations (18) through (20) under the above backward difference scheme:

$$\bar{A}\bar{A}_{i+1,j+1} = [(1 + F_1 - F_6 - F_1F_6 - F_2F_4)D_1 - F_2D_2 + (F_6 - 1)D_3]/(\text{DETERM}) \tag{18}$$

$$\bar{t}_{i+1,j+1} = [(F_3 + F_1F_3 - F_1F_4)D_1 + D_2 + (F_4 - F_3)D_3]/(\text{DETERM}) \tag{19}$$

$$\bar{v}_{i+1,j+1} = [(F_2F_3 - F_1 + F_1F_6)D_1 + F_2D_2 + (1 - F_6)D_3]/(\text{DETERM}) \tag{20}$$

where

$$(\text{DETERM}) = 1 + F_2F_3 - F_2F_4 - F_6 \tag{21}$$

$$D_1 = \bar{A}_{i,j} + \bar{v}_{i,j+1} \tag{22}$$

$$D_2 = \bar{t}_{i,j} \tag{23}$$

$$D_3 = F_1\bar{F} + \bar{v}_{i,j+1} \tag{24}$$

and F_1 through F_6 are equal to f_1 through f_6 multiplied by a constant difference increment $\Delta z = \Delta \tau$.

Referring to Figure 2, computation of transient solutions proceed in the following manner:

1. $\bar{F} = 0$, or thread tension equal to steady state value, is assumed;
2. Starting on $j = 2$, computation proceeds upward along the $j = 1$ line step by step using eqs. (18) through (20) until the take-up point $i = i_w$ is reached. This gives a tentative take-up speed $\bar{v}_{w1}$ which does not satisfy the boundary condition (17).
3. Step 2) above is repeated assuming a unity tension change $\bar{F} = 1$ giving another tentative take-up speed $\bar{v}_{w2}$ which also does not satisfy eq. (17).
4. The values of $\bar{F}$ which make the boundary condition (17) satisfied is given by the formula

$$\bar{F} = (1 - \bar{v}_{w1})/(\bar{v}_{w2} - \bar{v}_{w1}). \tag{25}$$

5. Step 2) is repeated using the $\bar{F}$ value given by (25) above.
6. Steps 1) through 5) are repeated for a desired number of times in time direction.

A computer program "MS3" having 355 FORTRAN statements was developed to carry out the above computation of transient solution in addition to the computation of steady-state solutions. It takes about 2 min on IBM 370/155 to compute the steady-state and transient solutions for one spinning condition.

Shown in Figures 3, 4, and 5 are steady-state thread thickness $A_0(x)$, steady-state thread temperature $t_0(x)$, and corresponding transient solutions for different air temperatures. It can be seen in Figure 5 that a high air temperature tends to make melt spinning unstable.

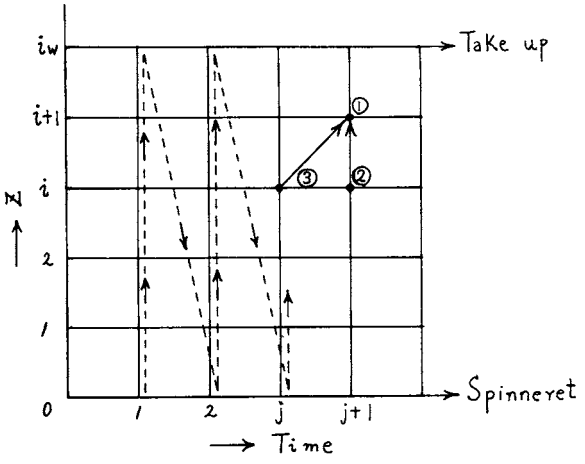

Fig. 2. Sequence of computation in the numerical solution of perturbation equations.

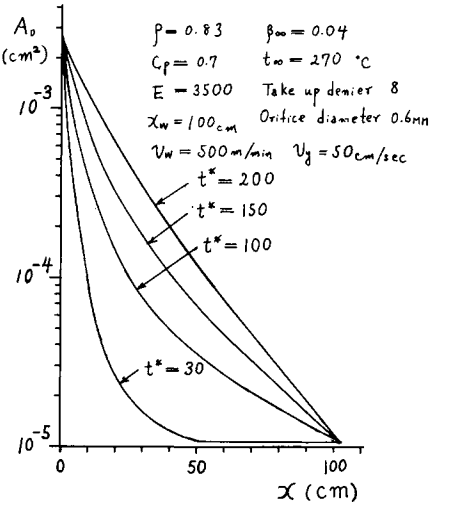

Fig. 3. Examples of steady state solution. Thread cross-sectional area A_0 vs. distance x.

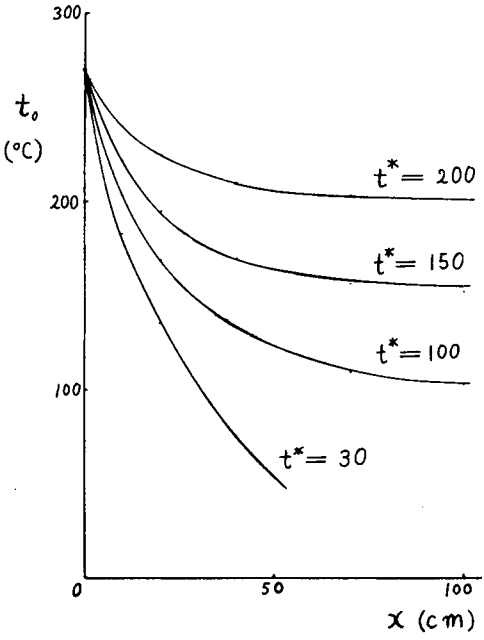

Fig. 4. Examples of steady-state solution. Thread temperature t_0 vs. distance x. Spinning conditions are same as in Fig. 3.

Analytical Solution of Perturbation Equations for the Isothermal Spinning

The steady-state solutions of eqs. (1) through (3) for the isothermal spinning are

$$v_0 = v_{00}e^{\alpha x} \tag{26}$$

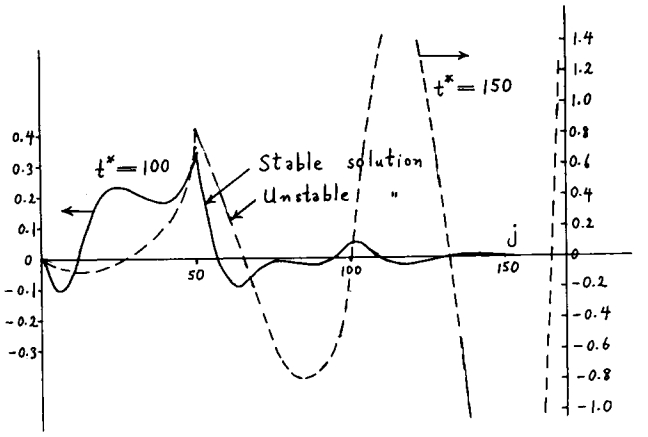

Fig. 5. Examples of transient solution. Spinning conditions are same as in Fig. 3.

$$A_0 = A_{00}e^{-\alpha x} \tag{27}$$

$$\alpha = \frac{1}{x_w} \log \frac{v_w}{v_{00}} \tag{28}$$

where subscripts 00 and w denote respectively the values at the spinneret and at the take-up point. In isothermal spinning, steady-state solutions are straight lines on semilog graph paper.

Perturbation equations (6) through (8) now become

$$\frac{\partial \bar{v}}{\partial z} = f_1(-\bar{A} - \bar{v} + \bar{F}) \tag{29}$$

$$\frac{\partial \bar{A}}{\partial \tau} = -\frac{\partial \bar{v}}{\partial z} - \frac{\partial \bar{A}}{\partial z} \tag{30}$$

$$f_1 = \frac{dv_0}{dx} = v_{00}\alpha e^{\alpha x} = \frac{1}{\dfrac{1}{v_{00}\alpha} - z}. \tag{31}$$

Equation (29) through (31) above can be integrated to give

$$\frac{\partial \bar{A}}{\partial z} = \frac{\phi(z - \tau)}{\dfrac{1}{v_{00}\alpha} - z} \tag{32}$$

where ϕ is an arbitrary function. If ϕ is equal to a unit step function,

$$\phi(z - \tau) = u(z - \tau) \tag{33}$$

a solution is obtained which represents the transient response of the isothermal spinning to a stepwise change in tension:

$$\bar{F} = -u(\tau) \tag{34}$$

$$\bar{A} = -\log (1 - \eta) \qquad (\eta < 1 - e^{-\xi}) \tag{35}$$

$$= \xi \qquad (\eta \geq 1 - e^{-\xi}) \tag{36}$$

$$\bar{v} = \frac{e^{-\xi}}{1 - \eta} - 1 + \log (1 - \eta) \qquad (\eta < 1 - e^{-\xi}) \tag{37}$$

$$= -\xi \qquad (\eta \geq 1 - e^{-\xi}) \tag{38}$$

where η and ξ are dimensionless variables defined as follows:

$$\eta = v_{00}\alpha\tau \tag{39}$$

$$\xi = -\log (1 - v_{00}\alpha z_w) = \log \frac{v_w}{v_{00}} = \alpha x_w. \tag{40}$$

Figure 6 shows the $\bar{A}$ and $\bar{v}$ values as given in eqs. (35) through (38). The curve

$$n = 1 - e^{-\xi} \tag{41}$$

in Figure 6 is the time measured in terms of η the polymer takes to flow down from the spinneret to the point ξ.

Since $\bar{A}$ and $\bar{v}$ given in eqs. (35) through (38) above are the response of thread thickness and thread velocity to a stepwise change in thread ten-

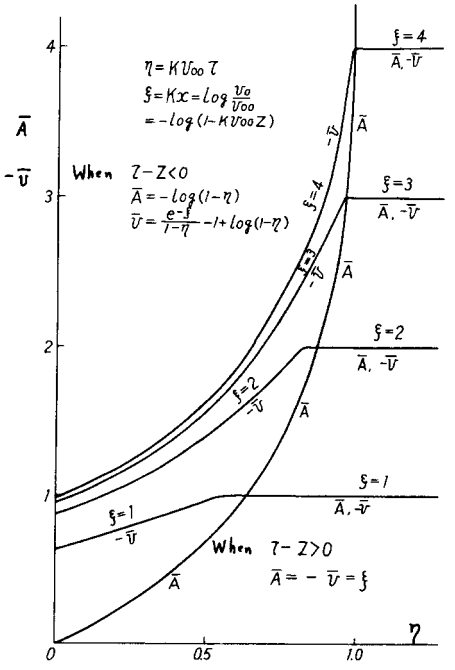

Fig. 6. Transient solution for a stepwise decrease in spinning tension.

sion, the response of thread thickness $\bar{A}$ to a unit step increase in thread velocity $\bar{v}$ can be expressed as

$$\bar{A}_w = L^{-1}\left[\frac{L[\bar{A}]}{L(\bar{v})}\frac{1}{s}\right] \tag{42}$$

where L [ ] and L^{-1}[ ] are respectively Laplace transform operator and inverse Laplace transform operator, and $\bar{A}$ and $\bar{v}$ on the right-hand side of the equation are those given in eqs. (35) through (38). $\bar{A}_w$ on the left-hand side of eq. (42) has a subscript w attached to it since the variable ξ can be interpreted to be the logarithm of the draw-down ratio between the spinneret and the take-up point. Above $\bar{A}_w$ is the desired transient solution that satisfies the boundary condition (17).

The vector loci of the denominator $L[\bar{v}]s$ in eq. (42) can be constructed by hand calculation and are shown in Figure 7. Values of angular frequency ω are marked on the vector loci; ω is given by the formula

$$s = j\omega \tag{43}$$

where j is $\sqrt{-1}$. Figure 7 shows that when ξ becomes more than 3.0, vector loci start to encircle the origin. This in turn makes the transient solution $\bar{A}_w$ given in eq. (42) contain an oscillation term growing exponentially with time, rendering the solution unstable. $\xi > 3.0$ is equivalent to

$$\frac{v_w}{v_{00}} = \text{draw-down ratio} = e^{\xi} > e^{3.0} = 20. \tag{44}$$

It follows, therefore, that an isothermal spinning is unstable when the draw-down ratio is more than 20. This fact was found independently by the author[4] and by Gelder.[10]

The value of ω at the intersection of the vector loci and the real axis is called the critical angular frequency ω_c and is approximately equal to the

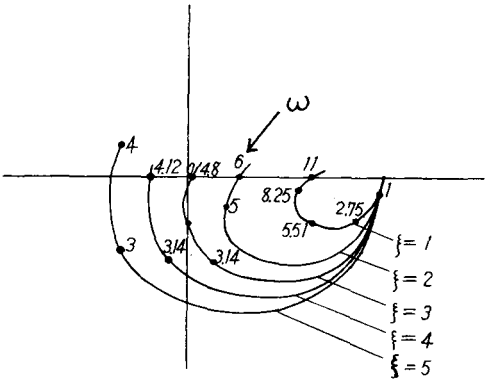

Fig. 7. Vector loci of $L[\bar{v}]s$.

angular frequency of draw resonance. ω_c is a function of ξ, and so is the dimensionless oscillation period η_c as shown in Figure 8:

$$\eta_c = \frac{2\pi}{\omega_c}. \tag{45}$$

The oscillation period of draw resonance, when expressed in the length of thread taken up, is then

$$x_c = \frac{v_w \eta_c}{v_{00}\alpha} = \frac{v_w}{v_{00}} \eta_c \frac{x_w}{\log \frac{v_w}{v_{00}}}. \tag{46}$$

The x_c is a function only of draw-down ratio v_w/v_{00} and air gap x_w.

STABILITY LIMITS

Parameters which affect the transient solution are coefficients f_1 through f_c in eqs. (6) through (8) and z_w, the value of z at the take-up point. All these values become fixed when the steady-state solution v_0, A_0, and t_0 are fixed. It follows then that the parameters affecting the stability are identical to the parameters that affect the steady-state solution.

A dimensional analysis on the steady-state version ($\partial/\partial\tau = 0$) of eqs. (1) through (3) reveals that these parameters can be grouped into the four dimensionless groups below:

$$\frac{E(t_{00} - t^*)}{(273 + t^*)^2} = \text{measure of temperature dependence of viscosity} \tag{47}$$

$$\mathrm{St} = 1.67 \times 10^{-4} \rho^{-0.334} C_p^{-1} G_0^{-0.666} A_{00}^{-0.167} x_w \tag{48}$$

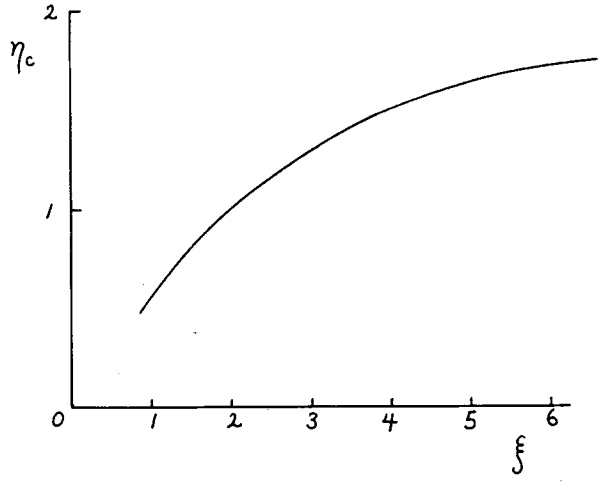

Fig. 8. Dimensionless oscillation period η_c vs. log of draw-down ratio.

$$\psi = \frac{v_{y0}}{v_{00}} = \text{dimensionless cooling air speed} \tag{49}$$

$$1/\lambda_w = \frac{v_w}{v_{00}} = \text{drawn-down ratio.} \tag{50}$$

By computing transient solutions under many different values in the above four dimensionless groups, and by classifying the solutions with respect to convergence with time, the stability limits can be obtained as closed surface in a four-dimensional space. Since, however, it takes too much computation time, draw-down ratio $1/\lambda_w$, activation energy E, and spinneret temperature t_{00} were given fixed values and the stability limits were expressed as curves on the (t^* — St) plane for two different values of ψ; t^* was used instead of $E(t_{00} - t^*)/(t^* + 273)^2$ for the convenience in visualizing and interpreting the role of cooling played in the stability of melt spinning.

The stability limits derived in this manner for spinning conditions I (Table I) are shown in Figure 9.

The dots and triangles marked on Figure 9 are the t^* — St combinations for which steady-state and transient solutions were computed, using program MS3, to draw the stability limits. The lowermost curve in Figure 9

TABLE I
Spinning Conditions I

E	3500 deg (for PP)
t_{00}	270°C
$1/\lambda_w$	264
ψ	0 and 9.15

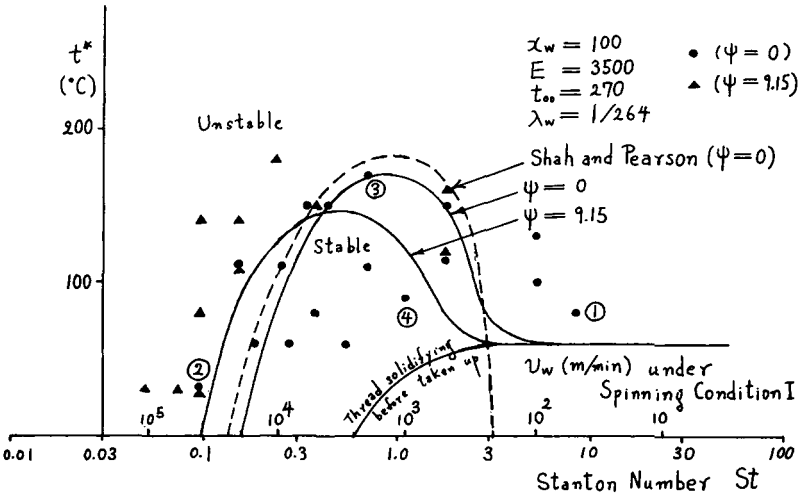

Fig. 9. Stability limits for spinning conditions I.

shows the boundary of the region in which the thread solidifies before it reaches the take-up point.

Shah and Pearson[6] have given the stability limits for Newtonian liquids as

$$S = \bar{k}\mathrm{Ste}^{-\mathrm{St}} \tag{51}$$

where S is a function of draw-down ratio $1/\lambda_w$ and is

$$S = 0.6 \qquad \text{for} \qquad 1/\lambda_w = 264. \tag{52}$$

Coefficient $\bar{k}$ above can approximately be expressed in terms of E, t^*, and t_{00} by the relation

$$\bar{k} = 5.55 \times 10^{-6} E(t_{00} - t^*). \tag{53}$$

Equation (51) through (53) and spinning conditions I combine to give

$$t^* = t_{00} - \frac{1.8 \times 10^5 \mathrm{Se}^{\mathrm{St}}}{E\mathrm{St}} = 270 - 31.3\,\frac{e^{\mathrm{St}}}{\mathrm{St}} \tag{54}$$

Equation (54) above is plotted in Figure 9 as the dotted curve which corresponds to the author's curve for $\psi = 0$.

Figures 10 and 11 are steady-state solutions corresponding to points 1 through 4 in Figure 9. The following are discussions of Figures 9 through 11.

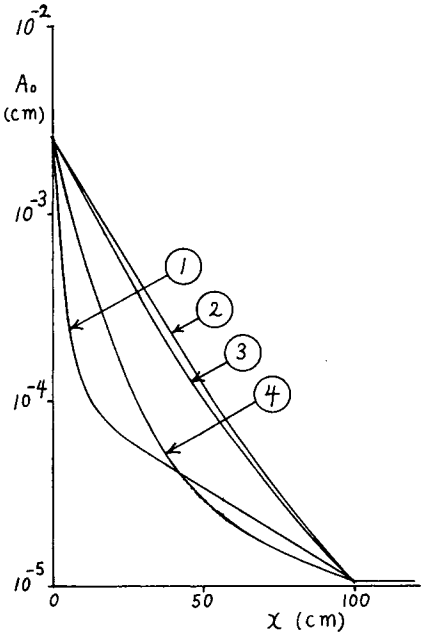

Fig. 10. Steady-state thread cross-sectional area vs. distance. Numbers 1 to 4 correspond to those in Fig. 9.

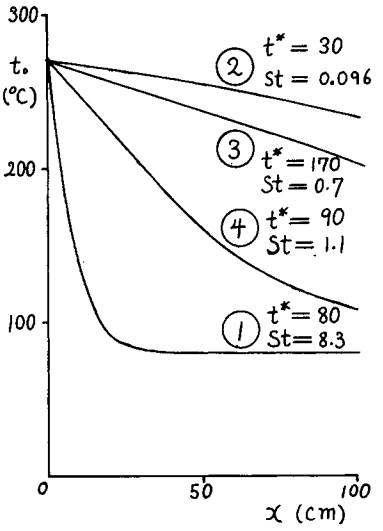

Fig. 11. Steady-state thread temperature vs. distance x. Numbers 1 to 4 correspond to those in Fig. 9.

1. The thread must be in a molten state at the take-up point before melt spinning can become unstable, since in Figure 9 the stable region completely contains the region in which the thread solidifies prior to take-up. Experimentally, a molten thread can not be taken up on a roll. Therefore, means for a quick quench such as water bath or chill roll must be provided between the spinneret and the take-up roll before draw resonance can start. Such a quick quench not accompanying drawn-down is irrelevant to the dynamics of melt spinning and may be considered to take the place of take-up point.

2. Conventional industrial melt spinning is always stable because threads solidify in air prior to take-up.

3. As the air temperature t^* rises, eventually the melt spinning becomes unstable.

4. Horizontal cooling air speed v_y (or ψ) shifts the stability limits toward lower St values. As a result, the cooling air speed has a stabilizing effect in the low St region and a destabilizing effect in the high St region.

5. The stability limits for $\psi = 0$ agrees well with the stability criterion given by Shah and Pearson, except in the region bounded by $St > 3$ and $t^* < 60$. This region corresponds to very slow spinning in cool air. Since such spinning naturally is stable, the author's curve is valid. The discrepancy comes from the fact that the complete solidification of the thread at low temperatures has not been taken into consideration by Shah and Pearson.

6. Steady-state solutions 1, 2, and 3 in Figures 10 and 11 are those of unstable spinning. The three solutions have one thing in common which the stable solution 4 does not have. That is to say, the former three solu-

tions are close to those of isothermal spinning either over the entire length of spinning way or over most of the spinning way except the neighborhood of the spinneret. Since an isothermal spinning under the present draw-down ratio of 264 is unstable as discussed before, it may be concluded that melt spinning becomes unstable when it approaches the state of isothermal spinning.

7. In the medium St range, the stability limits extend into high air temperatures. This is estimated to be due to the fact that the balance struck between cooling and spinning flow rate make the shape of steady-state solutions differ from that of an isothermal spinning.

8. In summary, the cooling of the thread in the air gap plays a predominant role in the stability of melt spinning as far as Newtonian liquids are concerned.

SIMULATION OF EXPERIMENTS

Water-quenched Melt Spinning of PET

A water-quenched melt spinning of PET was carried out. The spinning had the geometry shown in Figure 12. The thread was quenched almost instantly in a water bath placed 2 cm below the spinneret. Spinning conditions are shown in Table II. The last three values in Table II are computed using eqs. (48) through (50).

The water-quenched melt spinning spontaneously developed a clear-cut draw resonance, as shown in Figure 12. The maximum thickness reached as much as four times the minimum. Period of oscillation was 71.2 cm in terms of the length of thread taken up.

Thereafter, a cooling air current 60 cm/sec in speed was blown through the 2-cm air gap using a small blower. This surpressed the draw resonance bringing the spinning back to stability as the dotted curve in Figure 12

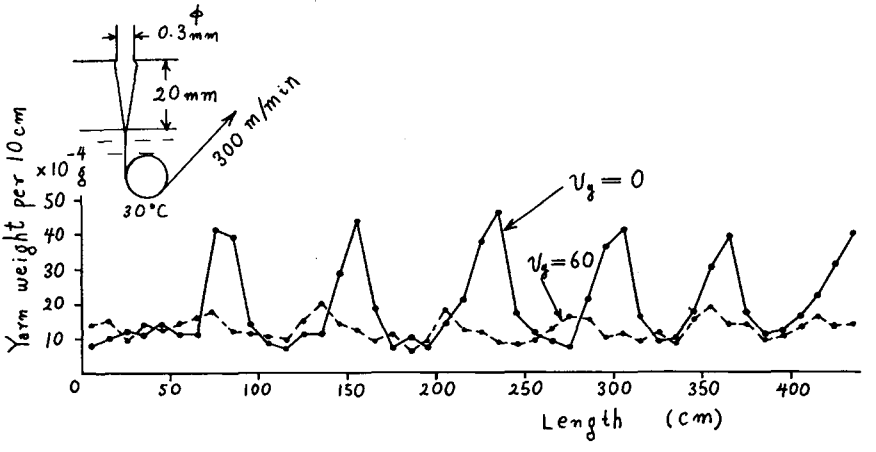

Fig. 12. Draw resonance encountered in a water-quenched melt spinning of PET.

shows. In what follows, the above two experiments are simulated by means of the theoretical model developed in the preceding sections.

Coefficient h_{H_2O} of heat transfer to water was derived using a handbook formula assuming that the thread diameter and the thread velocity were equal to those at the take-up, on the grounds that little draw-down of the thread was expected in the water bath. The h_{H_2O} value was found to be 3.12 cal/(cm^2 sec deg), being 176 times the corresponding value of h for heat transfer to air. Using parameter values in spinning conditions II and the above h_{H_2O} value, steady-state and transient solutions were computed by means of program MS3 as shown in Figure 13, 14, and 15. The solid curves

TABLE II
Spinning Conditions II

Spinneret orifice diameter	0.3 mm
Average take up denier	11.3
Spinneret temperature t_∞	284°C
Take-up speed v_w	300 m/min
Horizontal cooling air speed v_{y0}	0 and 60 cm/sec
Air temperature t^*	30°C
Water temperature	30°C
Specific gravity of polymer ρ	1.33 g/cm^3
Specific heat of polymer C_p	0.40 cal/(g deg)
Activation energy of polymer E	3240 deg
St	0.073
ψ	0 and 9.15
$1/\lambda_w$	76.2

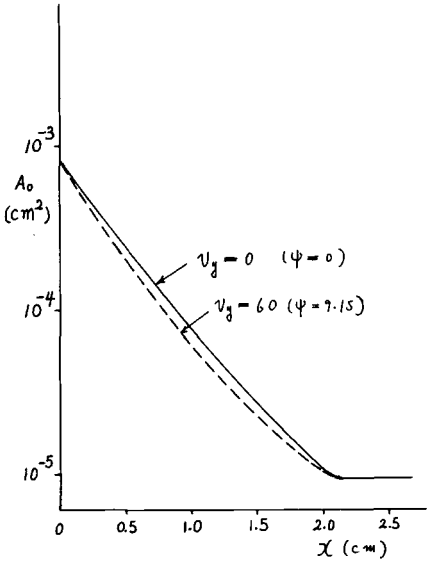

Fig. 13. Simulation of experiments. Steady-state solutions in thread cross-sectional area.

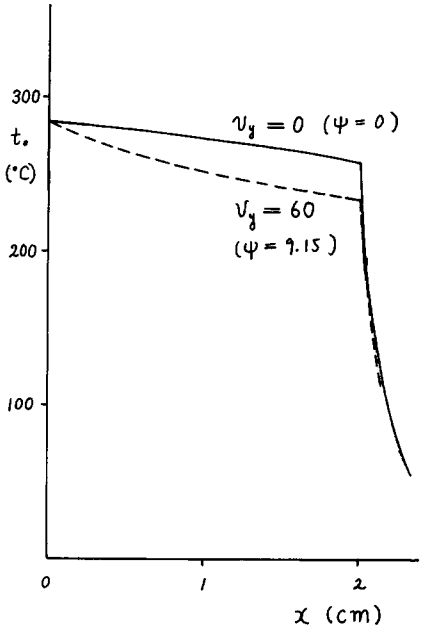

Fig. 14. Simulation of experiments. Steady-state solutions in thread temperature.

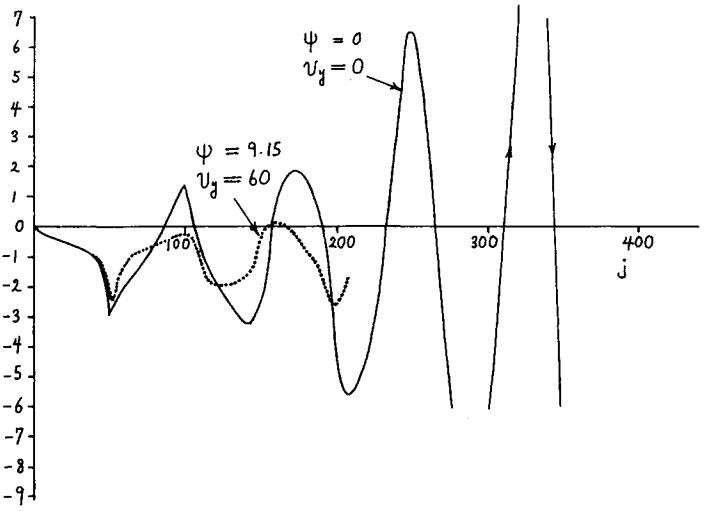

Fig. 15. Simulation of experiments. Transient solutions corresponding to Fig. 12.

are for $\psi = 0$ and the dotted curves are for $\psi = 9.15$. Figure 13 attest to the assumption that little draw-down of thread takes place in water bath.

The solid curve in Figure 15, a growing oscillation, is the simulation of the experimentally observed draw resonance shown as solid lines in Figure 12. The simulation is in agreement with experiment in that both are oscillatory and unstable. The experimental curve, however, is a standing

oscillation due to the nonlinearity of the physical system which is lost in moving from eqs. (1) through (3) to the perturbation equations.

The simulation in Figure 15 has an oscillation period of 80 in j. Since $j = 50$ is programmed to correspond to the time z_w the thread takes to flow down from the spinneret to the take-up point which in this case mathematically coincides with the water surface, the oscillation period when converted into the length L_c of the thread taken up computes as

$$L_c = \frac{80}{50} z_w v_w = 1.6 \times 0.0709 \times 300 \times (100/60) = 56.9 \text{ cm} \quad (z_w \text{ is } 0.0709 \text{ sec}). \quad (55)$$

The simulated oscillation period (55) is 20% less than the experimental value of 71.2 cm. Considering that the perturbation equations are meant for small deviations from the steady-state values and cannot fully cope with the fourfold thickness variation in Figure 12, the 20% discrepancy may be considered small enough.

The stabilizing effect of the cooling air found experimentally as shown in Figure 12 is also reflected in the theoretical curves in Figure 15 in that the curve for $\psi = 9.15$ is nearly stable while the curve for $\psi = 0$ is clearly unstable.

The theoretical stability limits drawn on the (t^* — St) plane in Figure 16 are compatible with spinning conditions II. Here again, the stabilizing effect of the cooling air is clearly demonstrated. Spinning conditions II, shown as a dot in Figure 16, are in the unstable region when ψ is 0, but they become enclosed in the stable region when ψ becomes 9.15.

The Casting of PP Film

The casting of plastic film is a kind of melt spinning having a two-dimensional flow pattern as shown in Figure 17. The melt is extruded

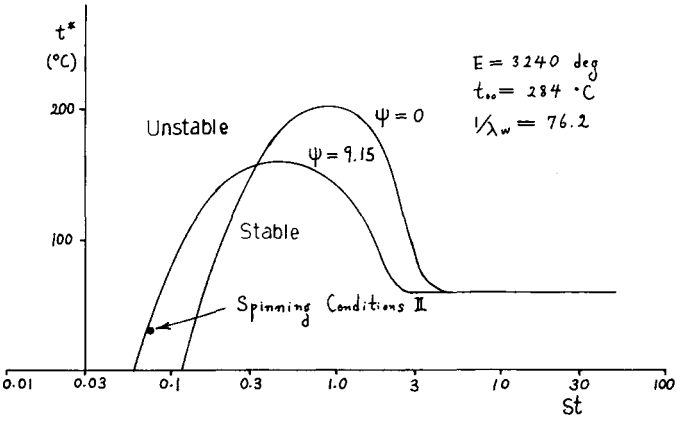

Fig. 16. Stability limits compatible with spinning conditions II showing the stabilizing effect of cooling air.

through the die, is drawn thin while running down the air gap, adheres to a chill roll while still in a molten state and is quickly quenched to solidification.

Draw resonances such as the ones shown in Figure 18 are often encountered in the casting of PP films. As discussed before in relation to the stability limits, this is due to the comparatively poor cooling of the film in the air gap.

Equation (1) through (3) of melt spinning are applicable to the casting of plastic film except that changes must be made on the right-hand side of eq. (3) as shown below, on account of the difference in geometry:

$$\frac{\partial t}{\partial \tau} + v \frac{\partial t}{\partial x} = \frac{2h^*(t^* - t)}{\rho C A} \tag{56}$$

where the variable A is the film thickness (cm) rather than the cross-sectional area, and the Trouton viscosity β is twice the value of shear viscosity μ rather than three times μ in fiber spinning. It is fairly difficult to make use of eq. (56) since the complex geometry and the presence of an

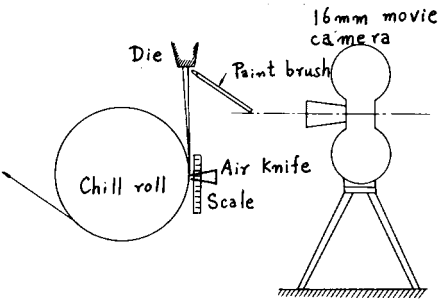

Fig. 17. Diagram of film casting and the measurement of film speed.

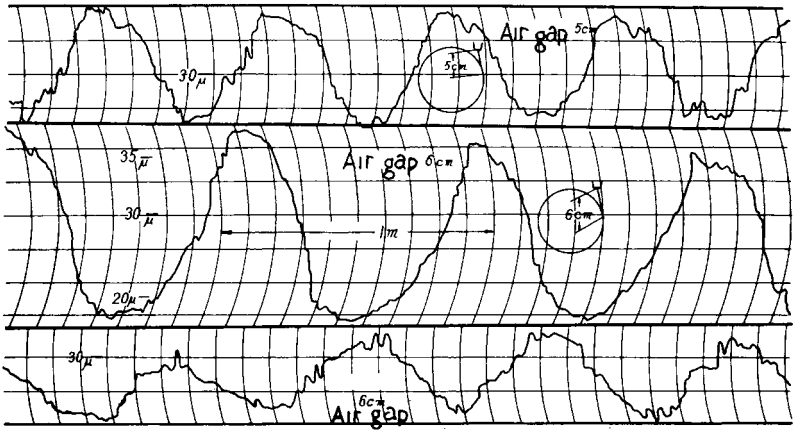

Fig. 18. Draw resonance encountered in the casting of unoriented PP film. Film thickness in machine direction measured by means of an electric capacitance-type micrometer.

"air knife" make it difficult to express the coefficient h^* of heat transfer in terms of operating conditions.

Fortunately, the casting of unoriented PP film was found to be close enough to the isothermal spinning so that the analytical solution for the isothermal spinning can be used to predict the oscillation period. To check on the closeness, the steady-state thickness, and temperature of the film were measured experimentally. An industrial film-casting machine was run under the conditions shown in Table III throughout the experiments unless specified otherwise.

Instead of directly measuring the film thickness, movement of paint specks marked on the film was measured by taking 16-mm movie pictures of the film as shown in Figure 17. Shown in Figure 19 are two displacement-versus-time curves read off the movie pictures. Graphic differentiation of the displacement curves gives film surface speed from which film thickness $A(x)$ can be derived as functions of distance x from the die. Film temperature $t(x)$ was measured by means of a zero balance-type contact thermocouple essentially identical to the one used on threads. Figure 20 shows $A(x)$ curves measured under two different throughputs. While the mea-

TABLE III
Film-Casting Conditions

Effective die opening A_{00}	1000 μ
Film thickness A_w	30 μ
Take-up speed v_w	30 m/min
Draw-down ratio $1/\lambda_w$	33
Air gap x_w	50 mm
Extruder motor speed	850 rpm

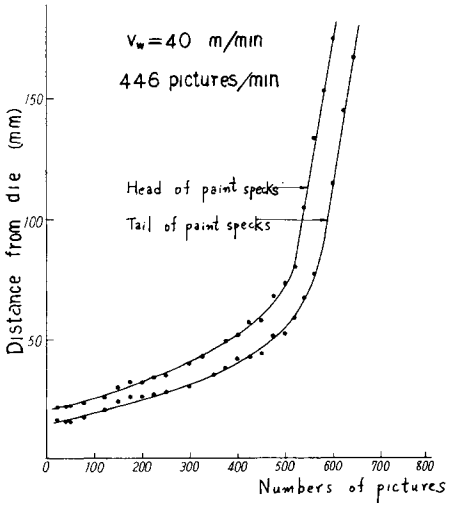

Fig. 19. Example of paint speck displacement.

sured $t(x)$ curve in Figure 21 shows a considerable cooling of the film in the air gap, the thickness curves in Figure 20 are approximately straight lines on the semilog graph paper exhibiting the trait of isothermal spinning. On account of this finding, an attempt was made to simulate the PP film casting by means of the analytical solution for the isothermal spinning discussed before.

Since the film-casting conditions were close to the stability limits, a sudden start of air knife always caused a damped oscillation in film thickness as the one shown in Figure 22, even when the casting was stable.

Oscillation periods were measured in this manner under different values of (i) take-up speed v_w, (ii) die exit speed v_{00}, and (iii) air gap x_w and shown as dots in Figures 23 through 25. The solid curves drawn on the same figures are the theoretical oscillation periods given by eq. (46). The theoretical values agreed very well with experimental values.

However, the theoretical simulation failed to agree with experiments in the stability as the transients in Figure 22 show. This is to be expected

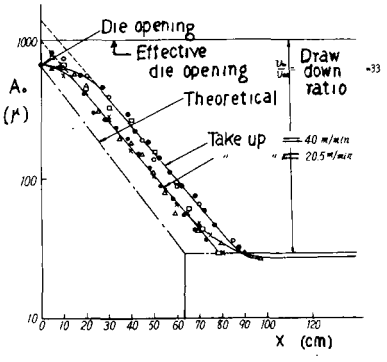

Fig. 20. Film thickness vs. distance from die derived from paint speck displacement curves.

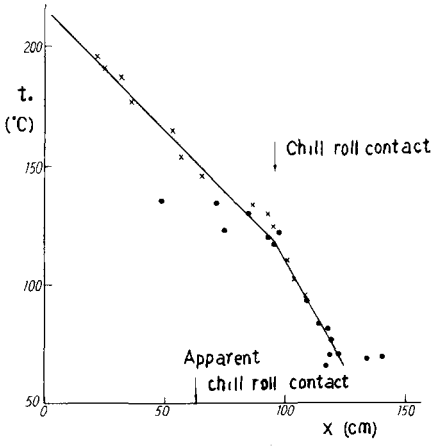

Fig. 21. Measured film temperature vs. distance from die.

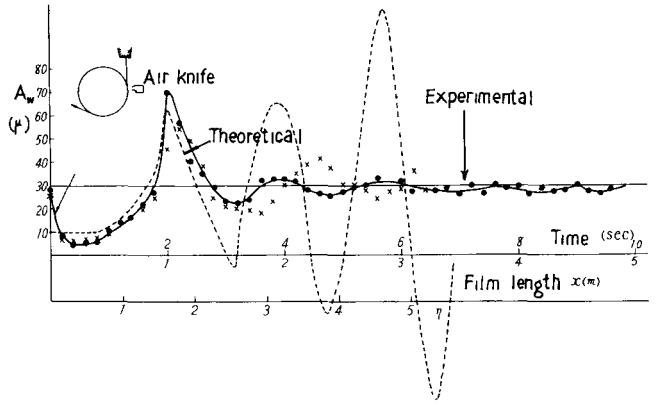

Fig. 22. Film thickness after a sudden stop of air knife, both experimental and theoretical.

because isothermal spinning is known to be unstable under the present draw-down ratio of 33 which is more than the critical value of 20. Evidently, eq. (56) must be taken into consideration before the stability limits can be accurately predicted.

Nevertheless, the very good agreement obtained on the oscillation periods is evidence enough for the basic validity of simulating the draw resonance in film casting by means of the present theoretical model.

Water-Quenched Extrusion of PP Ribbons

Bergonzoni et al.[9] observed the draw resonance encountered in the water-quenched extrusion of thick PP ribbons approximately 1 mm × 5 mm in cross section at the take-up. Figures 26 through 29 are reproduced from their report. Figure 26 shows the equipments used in their experiments; the air gap was 6 in. and 12 in.

Although no data are available on the take-up speed or mass throughput G_0, it is still possible to roughly estimate the St value in their experiments. Assuming a likely take-up speed of $v_w = 60$ m/min and a draw-down ratio of $1/\lambda_w = 20$, variables on the right-hand side of eq. (48) have the following values:

$$\rho = 0.83 \text{ g/cm}^3 \qquad C_p = 0.7 \text{ cal/(g deg)} \qquad \text{for PP}$$
$$A_{00} = 0.1 \text{ cm} \times 0.5 \text{ cm} \times 20 = 1 \text{ cm}^2 \qquad G_0 = 4.2 \text{ g/sec}$$
$$x_w = 12 \text{ in.} = 30.5 \text{ cm.} \tag{57}$$

Substituting these values into eq. (48), the St value computes as

$$\text{St} = 1.9 \times 10^{-3}. \tag{58}$$

This St value is one order of magnitude smaller than in the water-quenched melt spinning of PET discussed before. Since a small St means less cooling in the air gap, it can safely be assumed that the ribbon extrusion by Bergonzoni et al. was for practical purposes an isothermal spinning. Theories on isothermal spinning should, therefore, be applicable here.

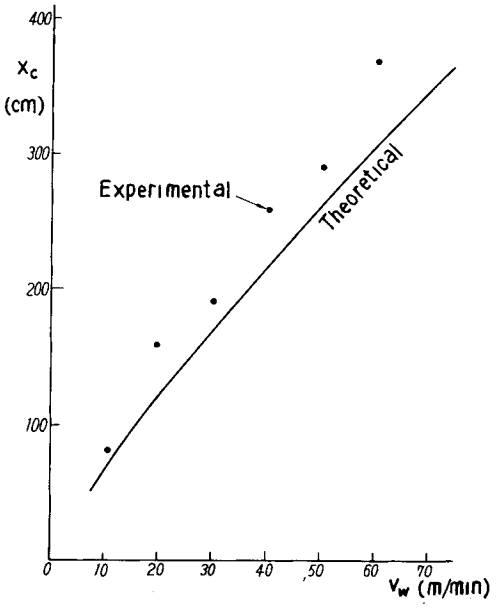

Fig. 23. Oscillation period vs. take-up speed, both theoretical and experimental (air gap = 12.5 cm, A_w = 30 μ at v_w = 30 m/min).

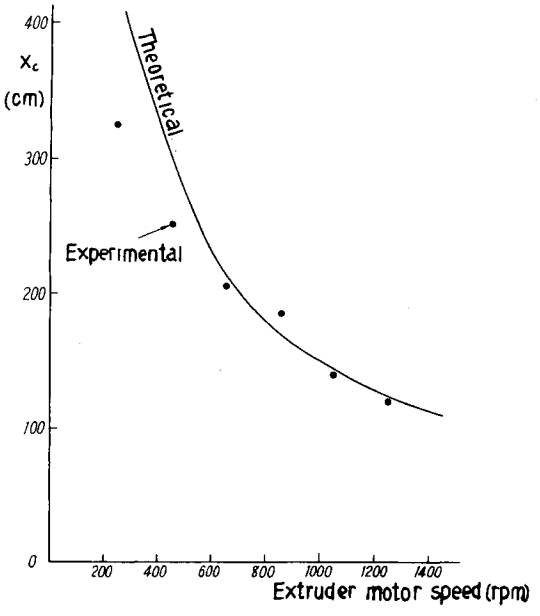

Fig. 24. Oscillation period vs. extruder motor speed, both theoretical and experimental (air gap = 12.5 cm, v_w = 30 m/min).

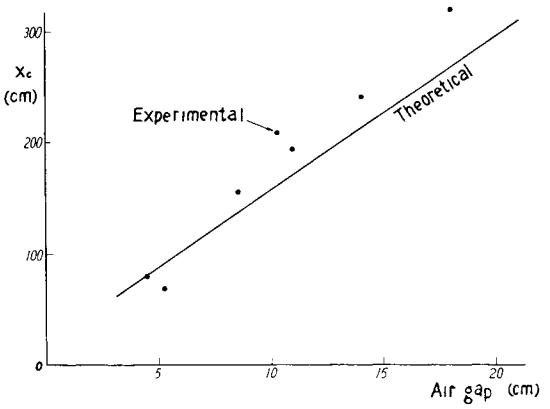

Fig. 25. Oscillation period vs. air gap, both theoretical and experimental (v_w = 30 m/min, extruder motor speed = 850 rpm).

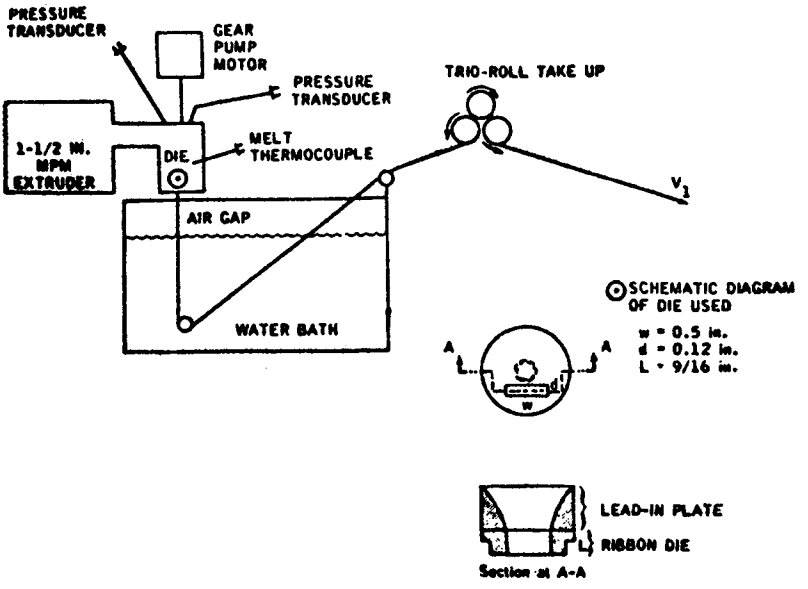

Fig. 26. Diagram of PP ribbon extrusion.

Shown in Figures 27 and 28 are the intensities of draw resonance expressed in terms of the ratio of maximum ribbon width over the minimum plotted with respect to the draw down ratio $1/\lambda_w$. Evidently, draw resonance started in the neighborhood of $1/\lambda_w = 20$, verifying the author's statement made in eq. (44).

Shown in Figure 29 is an example of draw resonance having an oscillation period of 92 in. in ribbon length. Referring to Figure 27, we know the

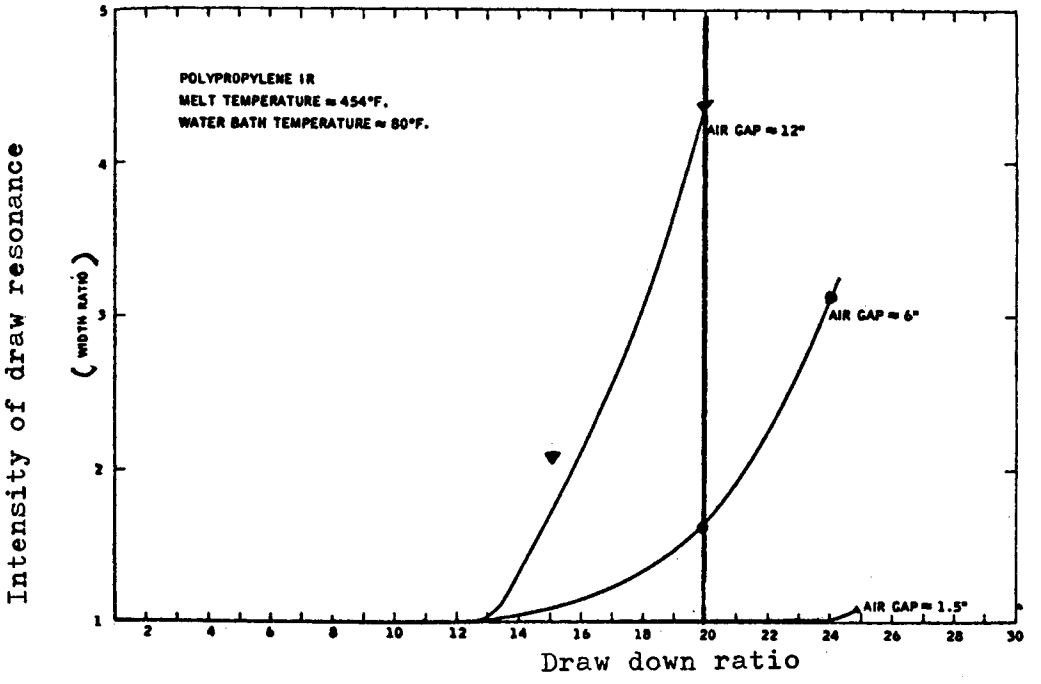

Fig. 27. Intensity of draw resonance vs. draw-down ratio under two different air gaps.

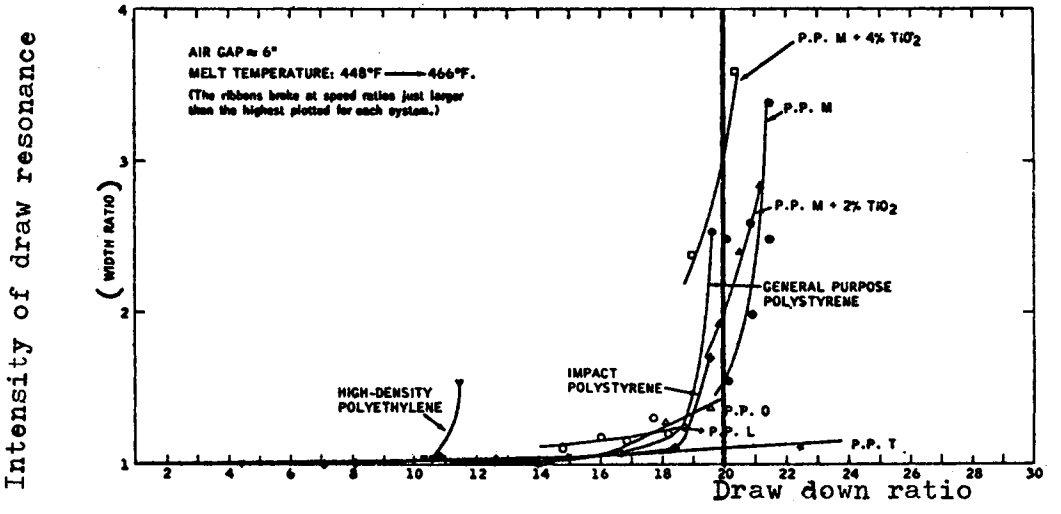

Fig. 28. Intensity of draw resonance vs. draw-down ratio for different polymers.

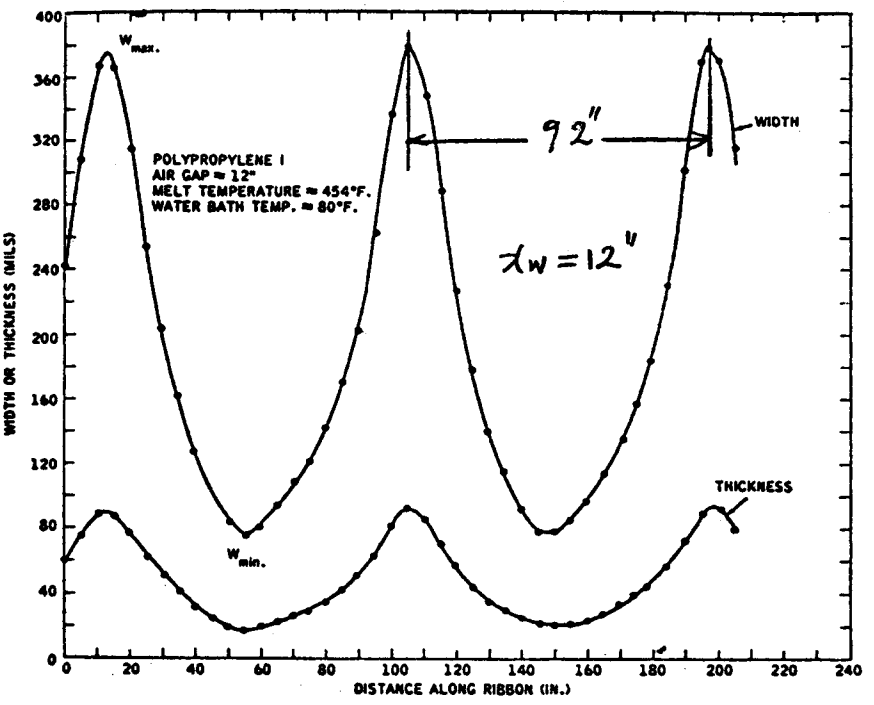

Fig. 29. Example of draw resonance in the extrusion of PP ribbon.

draw-down ratio $1/\lambda_w$ was 20, and as written in Figure 29, air gap x_w was 12 in. in this experiment. By substituting these $1/\lambda_w$ and x_w values into eqs. (40) and (46) and by referring to Figure 8, the theoretically predicted oscillation period is

$$x_c = \frac{1}{\lambda_w \log (1/\lambda_w)} \eta_c(\xi) x_w \tag{59}$$
$$= 20(1/3.0) \times 1.30 \times 12 \text{ in.} = 105 \text{ in.}$$

The above theoretical value is only

$$105 \text{ in.}/92 \text{ in.} = +14\% \tag{60}$$

larger than the experimentally observed value showing the close agreement between theory and experiment.

Figures 27 and 28 show, however, that in experiments draw resonance builds up gradually in the neighborhood of $1/\lambda_w$ rather than abruptly at $1/\lambda_w$. This difference is estimated to be due to (i) the non-Newtonian properties of polymer neglected in formulating eqs. (1) through (3), and to (ii) the loss of nonlinearity in taking the perturbations.

Conclusions

1. For the case of isothermal spinning, an analytical solution was obtained to the perturbed form of the partial differential equations of melt spinning developed by the author previously.

2. Isothermal spinning was found to be unstable when the draw-down ratio was more than 20.

3. Oscillation period of draw resonance in isothermal spinning was expressed as a function of draw-down ratio and air gap.

4. The stability limits for nonisothermal spinning were expressed in the form of diagrams in the (t^* − St) plane.

5. In nonisothermal spinning, cooling of the thread in the air gap plays a predominant role in stabilizing the spinning. Notably, the thread must be in a molten state at the take-up before instability can develop.

6. Instability develops when the spinning comes close to the state of isothermal spinning provided the draw-down ratio is more than 20.

7. The above theories agreed well with experiments on water-quenched melt spinning of PET and on the extrusion of PP ribbons in terms of oscillation periods and stability limits.

8. The analytical solution for isothermal spinning predicted closely the oscillation periods of draw resonance encountered in the casting of PP film.

In summary, mathematical models based on eqs. (1) through (3) provide adequate understanding of the causes of draw resonance in melt spinning.

The author wishes to express his sincere thanks to Dr. T. Matsuo, Mr. Y. Yoshimoto and Mr. H. Yasuda, all of Toyobo Co. Ltd., for their cooperation in this study.

References

1. J. C. Miller, *SPE Trans.*, 3, 134 (1963).
2. S. Kase and T. Matsuo, *J. Polym. Sci., A*, **3**, 2541 (1965).
3. S. Kase and T. Matsuo, *J. Appl. Polym. Sci.*, **11**, 251 (1966).
4. S. Kase, T. Matsuo, and Y. Yoshimoto, *Seni Kikai Gakkaishi* (*J. Japan Text. Mach. Soc.*), **19**, T63 (1966).
5. J. R. A. Pearson and M. A. Matovich, *Ind. Eng. Chem., Fundam.*, **8**, 605 (1969).
6. Y. T. Shah and J. R. A. Pearson, *Ind. Eng. Chem., Fundam.*, **11**, 145 (1972).
7. Y. T. Shah and J. R. A. Pearson, *Polym. Eng. Sci.*, **12**, 219 (1972).
8. Y. T. Shah and J. R. A. Pearson, *Ind. Eng. Chem., Fundam.*, **11**, 150 (1972).
9. A. Bergonzoni and A. J. DiCresce, *Polym. Eng. Sci.*, **6**, 45 (1966).
10. D. Gelder, *Ind. Eng. Chem., Fundam.*, **10**, 534 (1971).

Received March 11, 1974
Revised May 8, 1974